Craze structure and stability in oriented polystyrene

Claudio Maestrini
Montedipe Research Center, Via G. Taliercio 14, 46100 Mantova, Italy

and Edward J. Kramer*
Department of Materials Science and Engineering, Bard Hall, Cornell University, Ithaca, NY 14853 1501, USA
(Received 31 October 1989; revised 20 February 1990; accepted 20 February 1990)

Thin polystyrene (PS) films bonded to copper grids were oriented by straining them above T_g to an extension ratio λ_{or}. These films were strained at room temperature in directions parallel to and perpendicular to the initial orientation to produce 'parallel' and 'perpendicular' crazes, respectively. The crazes were examined by transmission electron microscopy and by optical microscopy in transmitted and reflected light. The craze extension ratio λ_{cr} decreases as $1/\lambda_{or}$ for parallel crazes and increases as $\lambda_{cr}^{1/2}$ for perpendicular crazes, in good agreement with the values expected from changes in λ_{max}, the maximum extension ratio of a strand in the entanglement network of the polymer glass. While the craze fibril diameter D increases with λ_{or} for parallel crazes and decreases with λ_{or} for perpendicular ones, the fibril spacing D_0 is independent of λ_{or}. A modification of the model of the fibril growth mechanism, involving the strain-hardening effects, is proposed to take into account the constancy of D_0 and the changes of the craze stress S_c with the orientation. Fragility test results demonstrate that fibril breakdown is the dominant step in craze fracture and that extreme perpendicular orientation strongly reduces the fibril breakdown strain.

(Keywords: crazing; craze extension ratio; molecular orientation; fibril growth mechanism; fibril stability)

INTRODUCTION

Crazes occur in many glassy polymers after yielding during tensile deformation. In isotropic polystyrene (PS) these crazes are microdefects which differ from cracks by the presence of many small polymer fibrils (diameter ~6–9 nm; volume fraction ~0.25) spanning from one craze–polymer interface to the other[1]. The role of crazes is very relevant to the fracture process: macroscopic cracks form by craze fibril breakdown and then propagate by further craze growth and fracture at the crack tip[2–9]. The plastic work controlled by craze growth and local fibril breakdown at the crack tip is the cause of the relatively high values of the critical strain energy release rate, G_{Ic}, measured for glassy polymers in fracture mechanics tests.

Many industrial manufacturing processes (i.e. injection moulding, extrusion, etc.) induce considerable molecular orientation in finished polymer articles and such polymers show a large degree of anisotropy in mechanical and fracture properties[10–15]. The anisotropy of G_{Ic} in oriented polymer glasses cannot be due to the rather small anisotropy of Young's modulus E[16–19], but rather must be ascribed to changes in the craze structure and breakdown process with the growth direction of the craze relative to the orientation axis.

Previous work demonstrated that, in fact, crazes in oriented polymers display different features that can explain the experimental G_{Ic} values. Beardmore and Rabinowitz[20] found that crazes form at higher stresses when the tensile axis is parallel to the molecular orientation direction M than when the axis was normal to M. In addition, fracture was found to occur at stresses above the minimum stress for crazing in all cases. Farrar and Kramer[21] demonstrated that the results of Beardmore and Rabinowitz could be interpreted in terms of craze morphology and structure. They concluded that, at the same level of tensile stress, the 'parallel' crazes, i.e. the crazes obtained when the tensile axis was parallel to the axis of molecular orientation M, are smaller and more numerous than the 'perpendicular' crazes, formed with the tensile axis normal to M. They also observed that λ_{cr}, the craze fibril extension ratio (inverse of the craze fibril volume fraction), was smaller for parallel crazes than for perpendicular crazes.

Donald and Kramer[22–25] subsequently developed a model describing the influence of molecular entanglements on the craze structure. This model suggests variations in the extension ratios of the fibrils in oriented polymers which are in qualitative agreement with the observations by Farrar and Kramer.

Low-angle electron diffraction studies of crazed polymers[26,27] and microscopic 'fragility' tests[28,29] have provided measures of the structural parameters of crazes (average fibril diameter, average fibril spacing, etc.) and of the statistical features relative to the phenomena of craze nucleation, local breakdown and fracture. However, these techniques have not been applied to the study of oriented materials.

A major problem has been to find a method of providing thin polymer films with reproducible orientation. Farrar and Kramer[21] cast films of polystyrene (PS) on high-molecular-weight polyethylene (PE) substrates,

* To whom correspondence should be addressed

0032-3861/91/040609-10

which were then drawn above T_g of the PS. However, on a microscopic scale, the PE deforms non-uniformly, producing a PS film of variable thickness with a rather rough surface; this film is also difficult to bond to the copper grid without relaxing the orientation.

One might imagine that it would be possible to bond the film to the copper grid first and then deform the grid and the film in tension at a temperature above T_g. Unfortunately the copper grid, when strained along the directions of the grid bars, fails at a tensile strain of less than 25%, thus severely limiting the degree of preorientation that can be achieved. However, if the grid is strained along a diagonal, much larger prestraining can be obtained without fracture of the copper, so that PS films with interestingly large degrees of preorientation can be produced.

The purpose of the present work is to use this new method of oriented film production to make detailed measurements of craze structure and morphology in oriented PS.

EXPERIMENTAL

The basic experimental technique described here is an adaptation of the one developed by Lauterwasser and Kramer[30]. Films were prepared from PS (Pressure Chemical Co.), which had a weight-average molecular weight, M_w, of 1800000 and a polydispersity index, M_w/M_n, of 1.15. Thin films of homogeneous thickness were produced on glass substrates by spin-casting from PS–toluene solutions. Before the spin-casting, the solutions were filtered using standard gel permeation chromatography (g.p.c.) filters (0.5 μm mesh size) in order to reduce the dust particle content. The film thickness was controlled by varying the PS concentration in the solution, holding the angular speed of the spin-caster constant.

After the spin-casting, the films were detached from the glass substrates by floating them on distilled water, from where they were picked up on pretreated copper grids whose geometry will be discussed in the following. The grid pretreatment consisted of an anneal at 700°C for 1 h to obtain fully softened copper followed by an immersion in a PS–toluene solution, from which polymer molecules were left onto the metal surface. Films deposited on these pretreated grids were exposed to benzene vapour, which swelled the polymer, thereby removing the wrinkles caused by the previous manipulations and causing the adhesion of the films to the PS-coated grids. The films were then dried for a period of 72 h at room temperature to allow the benzene to evaporate.

The molecular orientation was induced in the PS films in the following way. A temperature chamber was built from sheets of PS foam 2 in thick, which were coated with aluminium foil. The temperature chamber was heated with a 200 W infra-red bulb and the temperature, automatically adjusted by a temperature controller, could reach values higher than 150°C and stay constant, within a range of ± 1°C, for periods of time longer than 30 min.

Films and grids were mounted on motorized micrometers and put into the temperature chamber, then kept at 115°C for approximately 15 min to reach thermal equilibrium. At this point the grids were quickly strained in tension at a strain rate $\sim 10^{-2}\ s^{-1}$. Since the temperature was slightly higher than the T_g of PS the polymer molecules could orient during the straining without destroying the film integrity. In the following we refer to the strain and the extension ratio reached during the orientation process as ε_{or} and $\lambda_{or} = 1 + \varepsilon_{or}$, respectively. Different temperatures between T_g and 115°C and higher strain rates were also tried. However, for these conditions, film fracture or damage was always observed to occur during the orientation process. When the grids had reached the desired strain level, they were rapidly extracted from the chamber and cooled in a refrigerator to freeze the molecular orientation due to the strain above T_g.

Figure 1 shows the grids with the diamond geometry used in our experiments, before and after straining. These

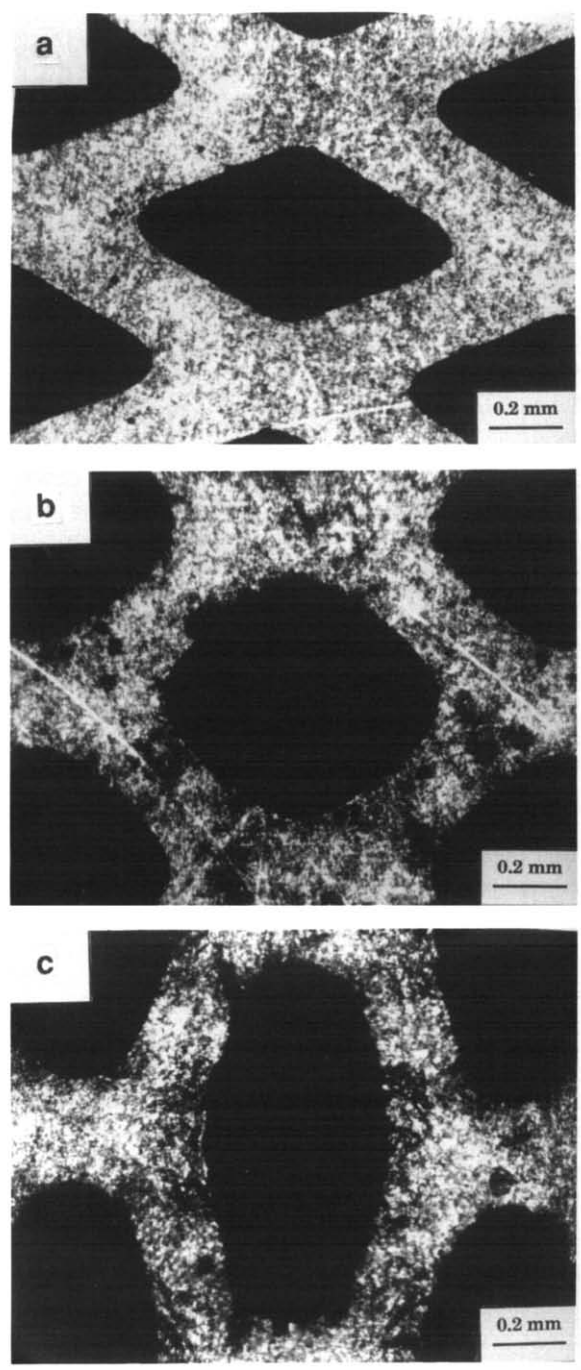

Figure 1 Copper grids used for the orientation experiments: (a) unstrained; (b) strain ~30%; (c) strain ~100%

new grids could be deformed to produce strains in an attached PS film that were greater than 60–70%. Nevertheless, especially for high strains, the deformation of the film was not completely homogeneous. For this reason, when possible, any measurement concerning the PS films was made in the central area of the diamond region.

The orientation took place above T_g so that the volume of the PS film in the diamond regions of the grids was constant during this deformation. Samples with constant final thickness are most appropriate for observations of the craze morphology and structure. These samples were prepared from PS–toluene solutions with concentrations that increased as the chosen degree of orientation increased to compensate for the thinning of the film during preorientation. On the other hand films were produced with constant initial thickness (before preorientation) intended for our statistical studies of craze nucleation, local breakdown and fracture, since in this case the constancy of the volume of polymer in each grid diamond simplifies the interpretation of the results.

After the orientation process, films and grids were ready for further tensile deformation at room temperature and low strain rates. Crazes appear in the oriented PS films during this low-temperature straining process. Following Farrar and Kramer[21] we use the terms 'parallel crazes' and 'parallel samples' for those obtained by straining the oriented films in a direction parallel to the orientation axis M. 'Perpendicular crazes' and 'perpendicular samples' are those which form when the films are strained in the direction normal to M.

RESULTS AND DISCUSSION

Craze structure and morphology

Oriented films with the same final thickness of about 0.4–0.5 μm were strained in tension at room temperature in the directions both parallel and perpendicular to the molecular orientation axis with strain rate of the order of $5 \times 10^{-7}\,s^{-1}$ until mature unbroken crazes were present in the film. Generally the crazes nucleated at the edges of the grids from natural defects and/or flaws in the polymer. For this reason craze nucleation occurred simultaneously in different regions and many crazes could be observed in the same diamond portion of the film.

For the purpose of the present paper, particularly in order to obtain low-angle electron diffraction (LAED) patterns, it was necessary to have large crazes in which the fibrillar structure covered at least an area of 20 μm in diameter. Following the procedure used by Yang and Kramer[27], artificial microcracks were introduced in the oriented polymer films by burning narrow holes with a length of about 120 μm in the direction perpendicular to the subsequent straining direction by using the focused beam of an electron microprobe. In this manner it was always possible to nucleate and grow crazes from the tips of these artificial microcracks which were sufficiently large. Individual diamonds could be cut from the deformed copper grid using a razor blade without changing the strain in the crazed film. These individual diamonds were immediately observed using a 200 keV JEOL transmission electron microscope to prevent coalescence of the fibril structure[27]. For each sample many micrographs of regions containing undamaged film, crazes and holes were taken, and LAED patterns of the same regions were obtained by switching the microscope to high-dispersion diffraction mode[27]. The TEM micrographs and the LAED patterns were then analysed using an optical microdensitometer.

Following Lauterwasser and Kramer[30] the values of the extension ratios of the fibrils inside the crazes λ_{cr} were calculated using the formula:

$$1/\lambda_{cr} = 1 - [\ln(\phi_{cr}/\phi_f)/\ln(\phi_h/\phi_f)] \qquad (1)$$

where ϕ_{cr}, ϕ_f and ϕ_h are respectively the optical densities of regions in the micrographs containing crazes, unbroken film and holes. The values of λ_{cr} obtained for the oriented samples were approximately constant at various positions along the crazes, with the exception of highly oriented perpendicular crazes ($\lambda_{or} \geq 1.4$), demonstrating that the mechanism of growth by surface drawing, which is predominant in unoriented PS crazing[30,31], is still active in the oriented material. Nevertheless the appearance of crazes is different depending on the orientation direction: *Figure 2* shows two micrographs of crazes in films with very different degrees of preorientation (parallel and perpendicular). As one can easily see great changes in the fibril extension λ_{cr} (estimable qualitatively by the contrast of the micrograph), fibril and midrib size had taken place.

Previous work[22–25] has demonstrated that in many glassy polymers λ_{cr} is strictly influenced by the properties of the entanglements of the macromolecular network. In

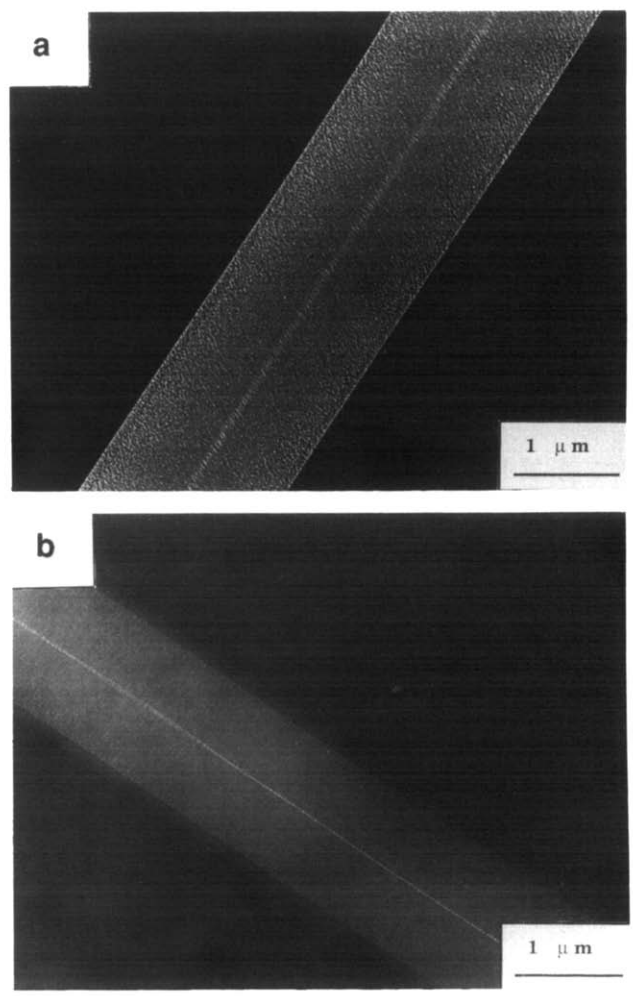

Figure 2 Transmission electron micrographs of crazes in oriented films: (a) perpendicular sample ($\varepsilon_{or} \sim 40\%$); (b) parallel sample ($\varepsilon_{or} \sim 40\%$)

essence it has been verified that, for a large number of polymers including PS, the value of λ_{cr} is very close to λ_{max} of a single strand in the entanglement network, where λ_{max} is:

$$\lambda_{max} = l_e/d \quad (2)$$

with l_e the chain contour length between entanglements and d the entanglement mesh size, i.e. the straight-line distance between entanglements.

Changes in λ_{cr} in oriented polymers could be expected since the molecular orientation obtained above T_g produces changes in λ_{max}. Consider a polymer melt extended in uniaxial tension to $\lambda_3 = \lambda_{or}$, $\lambda_2 = \lambda_1 = \lambda_{or}^{-1/2}$, where λ_1, λ_2 and λ_3 are the extension ratio coordinates in the directions perpendicular and parallel to the deformation, respectively. After the orientation, assuming no change for l_e during the deformation process, λ_{max} will be different for the parallel ($\parallel$) and perpendicular ($\perp$) directions as given by[1]:

$$\lambda_{max}(\parallel) = \lambda_{max}(\text{unor})/\lambda_{or} \quad (3)$$

$$\lambda_{max}(\perp) = \lambda_{max}(\text{unor})\lambda_{or}^{1/2} \quad (4)$$

Equations (3) and (4) can be rewritten in terms of λ_{cr}:

$$\lambda_{cr}(\parallel) \sim \lambda_{cr}(\text{unor})/\lambda_{or} \quad (5)$$

$$\lambda_{cr}(\perp) \sim \lambda_{cr}(\text{unor})\lambda_{or}^{1/2} \quad (6)$$

Experimental results obtained by Farrar and Kramer for one very large λ_{or} are qualitatively in agreement with (5) and (6), but no quantitative account of the relationship λ_{cr} and the extension ratios during the orientation process was reported in their work.

Figure 3 shows a plot of λ_{cr} *versus* λ_{or} for both parallel and perpendicular crazes in our samples. The full curves represent the formulae (5) and (6) which, within experimental error, are in good agreement with the measured values. *Figure 3* also shows a comparison, obtained only for parallel crazes, between data from samples with natural defects and/or flaws and samples with artificial microcracks. As one would expect, the experimental values of λ_{cr} do not depend on the size and nature of the defects present in the film. The same comparison was not made for perpendicular crazes, since in this case only the samples with artificial holes were analysed. Perpendicular crazes grew from natural defects at relatively larger strains than those from the artificial microcracks and were characterized by a very irregular geometry. These crazes were very brittle and quickly degenerated into quasi-macroscopic cracks not suitable for observation.

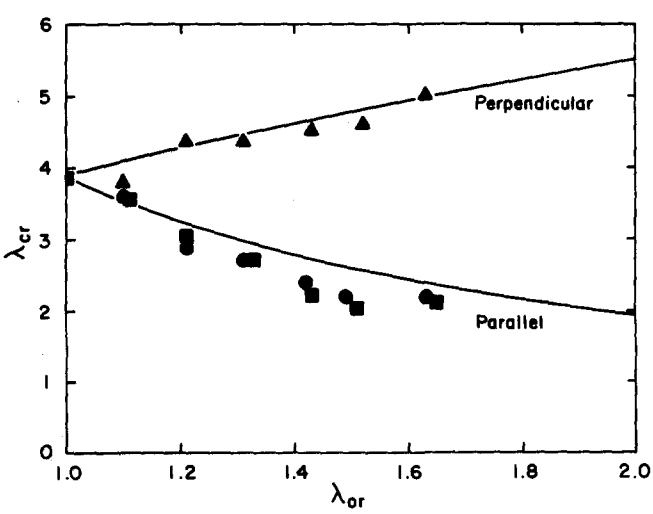

Figure 3 Craze extension ratio λ_{cr} as a function of the preorientation extension ratio λ_{or}: (▲) perpendicular samples with artificial microcracks; (■) parallel samples with natural defects and/or flaws; (●) parallel samples with artificial microcracks

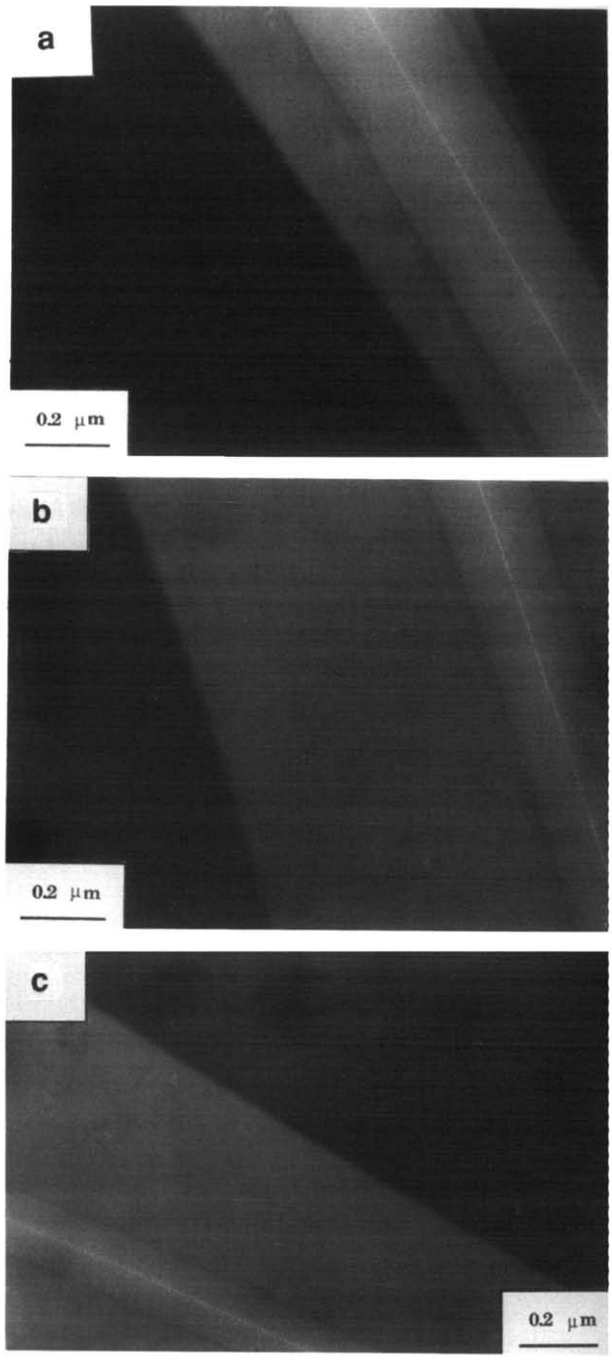

Figure 4 Transmission electron micrographs showing shear deformation zones at the edges of the crazes in parallel samples: (a) $\varepsilon_{or} \sim 40\%$; (b) $\varepsilon_{or} \sim 50\%$; (c) $\varepsilon_{or} \sim 60\%$

In parallel samples deformed unfibrillated zones at the interface between bulk polymer and craze were observed for values of λ_{or} higher than 1.3–1.4 (typical examples are shown in *Figure 4*). In highly oriented parallel samples ($\lambda_{or} > 1.5$), the craze portion in these uniformly deformed regions is very small and poorly defined. We concluded that those zones, whose appearance is very similar to that of shear deformation zones in other polymers[32,33]

are portions of the material in which a transition between the mechanisms of crazing and shear yielding occurred.

The TEM measurements of λ_{cr} do not provide any information about the microscopic structure of the crazes. The overlapping nature of the fibril structure made it impossible to resolve the single fibrils and analysis of the LAED patterns was necessary to obtain data on the average fibril diameter D, the average fibril spacing D_0 and the spatial arrangement of the fibril network. All the micrographs of the LAED patterns were recorded using a camera length of 62.8 m as measured by a calibration test using a carbon waffle grating with a lattice distance of 416 nm. *Figure 5* shows a typical optical microdensitometer trace of a LAED diffraction pattern in the direction parallel to the fibril scattering streak.

The analysis of similar patterns was performed for the oriented samples following the method of Porod[34,35] as applied to crazes by Brown[26]. The average fibril spacing D_0 was computed simply as the inverse of s_{max}, where s_{max} is the magnitude of the scattering vector s (defined as $s = 2\theta/\lambda$ with 2θ and λ the scattering angle and wavelength of the electrons, respectively) at the relative maximum in the graph of the optical density from the LAED pattern as shown in *Figure 5*.

The average fibril diameter D was obtained from the two scattering invariants k_i and Q. For scattering vector values $s > s_{max}$ the Porod law applies:

$$i(s) = k_i/s^3 + i_B \tag{7}$$

where $i(s)$ is the slit smeared intensity, i_B the background intensity (assumed to be independent of the fibril scattering[27]) and k_i the Porod's constant. The constant k_i and the background intensity i_B can be easily calculated from each densitometric trace by arranging the experimental data in the so-called Porod plot[27], which is a plot of $i(s)s^3$ *versus* s^3, and performing a linear regression. The value of i_B comes from the resulting slope and k_i from the y intercept. The LAED invariant Q is given by:

$$Q = 2\pi \int_0^\infty [i(s) - i_B]s\,ds \tag{8}$$

The integral in (8) can be split as follows as:

$$Q = \int_0^{s_e} [i(s) - i_B]s\,ds + \int_{s_e}^\infty [i(s) - i_B]s\,ds \tag{9}$$

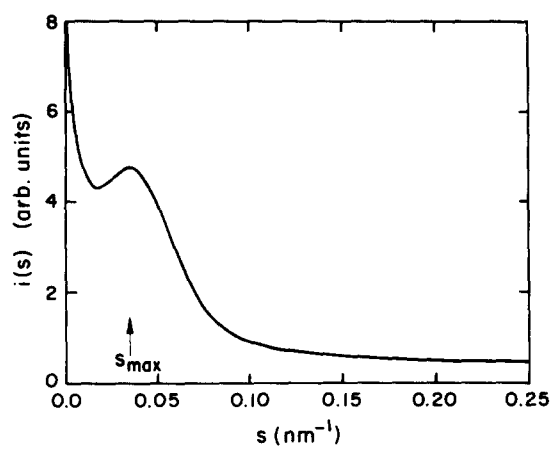

Figure 5 Typical plot of the low-angle scattered intensity $i(s)$ *versus* the scattering vector s for a LAED pattern scanned along the fibril scattering streak

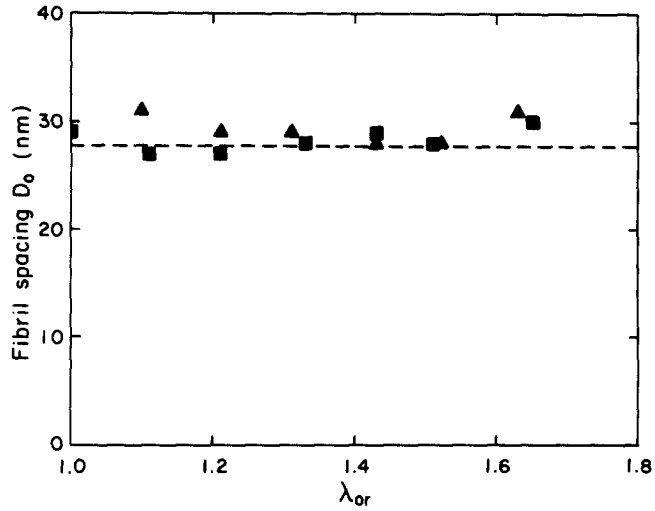

Figure 6 The average fibril spacing D_0 *versus* the preorientation extension ratio λ_{or}: (■) parallel samples; (▲) perpendicular samples

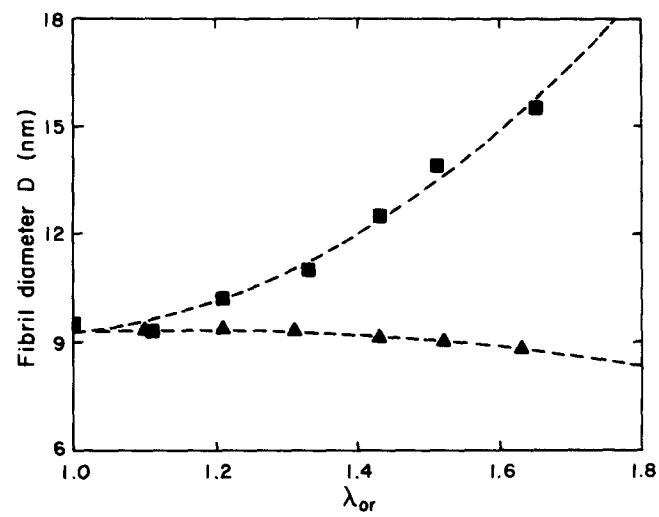

Figure 7 The average fibril diameter D *versus* the preorientation extension ratio λ_{or}: (■) parallel samples; (▲) perpendicular samples

where s_e is an arbitrary scattering vector far greater than s_{max} but inside the range of the experimental observations. The first of the two integrals in (9) is numerically computable from the experimental data, and, taking into account (7), the second one becomes:

$$\int_{s_e}^\infty [i(s) - i_B]s\,ds = \int_{s_e}^\infty \frac{k_i}{s^2}\,ds = \frac{k_i}{s_e} \tag{10}$$

where k_i has been previously computed from the same data. Finally the average diameter D is given by:

$$D = Q/[\pi^3 k_i(1 - 1/\lambda_{cr})] \tag{11}$$

where λ_{cr} is the value from the corresponding TEM measurements.

Figures 6 and *7* are respectively plots of D_0 and D *versus* λ_{or} for both the parallel and perpendicular crazes. The fibril diameter D varies from a value of about 9 nm for unoriented samples to a value of 15 nm in parallel crazes and 7 nm in perpendicular crazes. On the other hand the fibril spacing D_0 stays approximately constant for all the samples and has a value of about 30 nm.

Independent data from LAED patterns and TEM micrographs can be cross-checked by taking into account

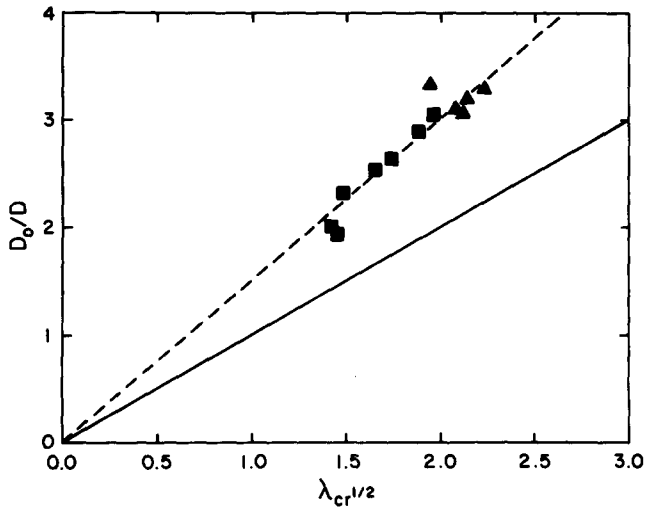

Figure 8 The ratio D_0/D as a function of $\lambda_{cr}^{-1/2}$. (■) parallel samples; (▲) perpendicular samples. The full line represents the theoretical expression $D_0/D = \lambda_{cr}^{-1/2}$ and the broken line the best experimental fit (slope ~1.5)

the fact that, from basic geometrical considerations, the following relation between D, D_0 and λ_{cr} must be true[1]:

$$D_0/D = \lambda_{cr}^{1/2} \tag{12}$$

Figure 8 shows the plot of the experimental ratio D_0/D *versus* $\lambda_{cr}^{1/2}$, and the full line represents the theoretical expression. The best linear fit to the experimental D_0/D is about 1.5 times greater than the expected value of $\lambda_{cr}^{1/2}$. This result can be explained by the fact that D_0, calculated as s_{max}^{-1}, is an overestimation of the real fibril spacing because of the large distribution in fibril diameter[26,27]. Assuming that the fibril diameter distribution is the same in all our samples and putting:

$$D_0^{(m)} = s_{max}^{-1} = cD_0 \tag{13}$$

where $D_0^{(m)}$ and D_0 are respectively the measured value and the real value for the average fibril spacing and c a constant greater than 1, (13) becomes:

$$D_0^{(m)}/D = c\lambda_{cr}^{1/2} \tag{14}$$

which is in good agreement with our experimental results if we take $c \sim 1.5$.

Parallel and perpendicular crazes also show different features with respect to the spatial arrangement of craze fibrils. As first suggested by Miller and Kramer[36,37], during the formation of the fibril surface several polymer strands may be strongly stretched on the void interface simultaneously, so that they cannot be broken. In this case a cross-tie fibril connecting two neighbouring main fibrils will appear and, because of the subsequent stress relaxation, this cross-tie fibril will exert a small force that displaces the main fibrils laterally, tilting them from the direction perpendicular to the craze surface. This lateral displacement and tilt can be detected and roughly measured from the LAED patterns[36,37].

Figure 9 shows three different LAED patterns taken respectively from a craze in a perpendicular sample, a craze in an unoriented sample and a craze in a parallel sample. As one can easily see for crazes in perpendicular and unoriented samples, a splitting between the lateral lobes of the LAED pattern is evident. This splitting signifies that the fibrils in the crazes have two main orientations differing by an angle δ, i.e. that a tilting due to the presence of cross-tie fibrils is present in the main fibril network. The angle δ, estimated from the LAED pattern, changes from about 20–25° for highly perpendicular crazes, to about 10° in unoriented samples, and it almost disappears in parallel samples, suggesting that many cross-tie fibrils are present in perpendicular crazes and that they are quite absent in parallel ones. This result is clearly understandable on the basis of the following simple considerations. When perpendicular crazes form, a large number of PS molecules are oriented in the direction normal to the main fibrils and are stretched along the strong carbon–carbon bonds. Thus there is

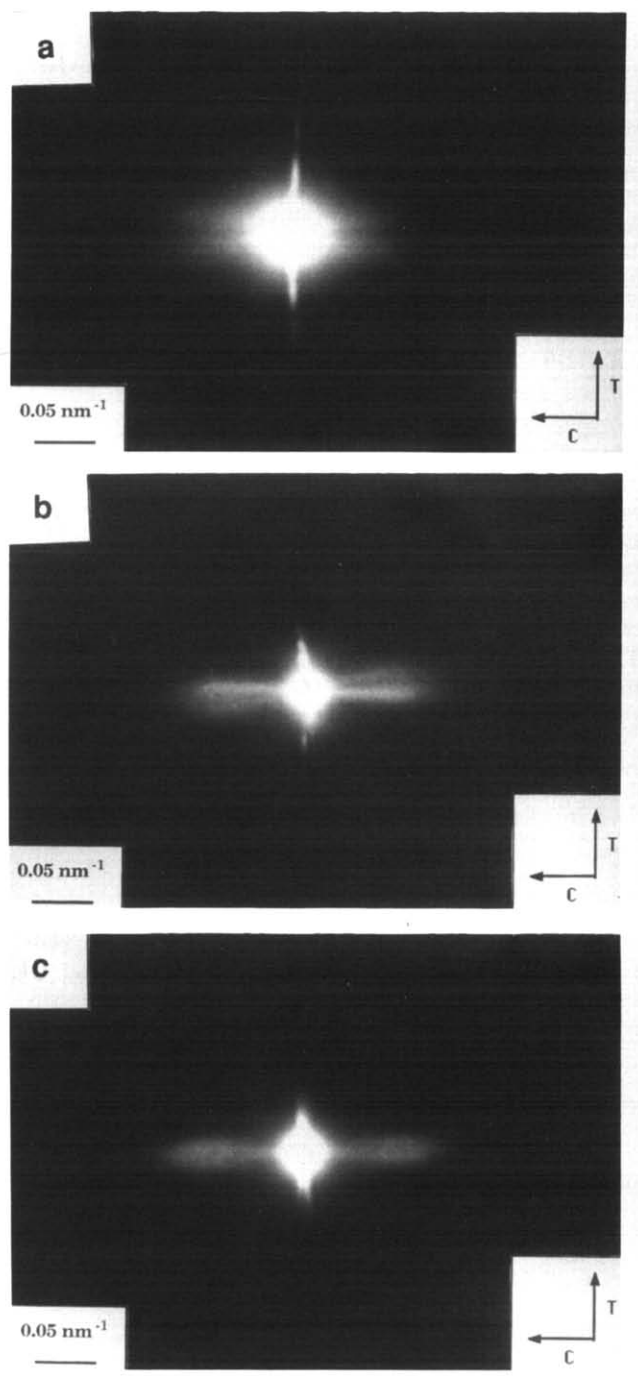

Figure 9 LAED patterns from crazes in oriented samples: (a) perpendicular sample ($\varepsilon_{or} \sim 50\%$); (b) unoriented sample; (c) parallel sample ($\varepsilon_{or} \sim 50\%$). The two axes T and C indicate the directions of the tensile axis and of the craze–bulk interface, respectively. The vertical streaks are due to refraction from the craze–bulk interface

a great probability that the interface by-passes bundles of molecules, forming numerous cross-tie fibrils. For parallel crazes the cross-tie fibrils are less numerous and weaker because the large majority of the macromolecules in the network are oriented along the main fibrils.

The data obtained allow us to give a graphic representation of the crazes in PS with different degrees of orientation. *Figure 10* shows a two-dimensional sketch of what a craze should look like in different orientation conditions.

The results presented in this section suggest that the model describing the fibril growth in the craze as a non-Newtonian flow process, first proposed by Kramer[1] for crazing in unoriented PS, should be modified in the presence of the orientation. In fact the standard non-Newtonian model implies that:

$$S_c = 8\Gamma/(\beta D_0) \tag{15}$$

where S_c is the macroscopic craze stress, Γ the surface energy for craze formation and β a constant smaller than 1. Taking into account that there is no reason to think that Γ could change with the orientation and that D_0 has been shown to stay approximately constant, one should conclude from (15) that S_c does not depend on the orientation either. However, strong evidence of the dependence of S_c on the orientation exists: Beardmore and Rabinowitz[20] showed that S_c increases in parallel samples and decreases in perpendicular samples. In addition the occurrence of shear deformation zones in highly oriented samples implies that S_c, in this case, must be higher than the shear yield stress and thus certainly higher than the corresponding S_c in unoriented samples.

We think that the inadequacy of the model in explaining data from oriented samples lies in the fact that the strain-softened polymer at the craze–bulk interface has been idealized as a fluid in which the strain-hardening effects are absent[1]. Argon[38] has suggested previously that one can divide the flow stress of the glassy polymer into a 'lossy' non-Newtonian viscous portion and a 'non-lossy' orientation hardening portion or 'back-stress'. Idealizing the polymer as a non-strain-hardening fluid amounts to neglecting this back-stress component.

The strain-hardening effects can be introduced in the existing model in the following way: the gradient of the hydrostatic tension $\nabla\sigma_0$ at the craze–bulk interface is given by[1]:

$$\nabla\sigma_0 \sim 2[(\sigma_0)_m - (\sigma_0)_s]/D_0 \tag{16}$$

where $(\sigma_0)_m$ and $(\sigma_0)_s$ are the effective hydrostatic tensions in the layer directly above the fibril and at the surface of the void 'ceiling' between fibrils, respectively. The hydrostatic tension at the void surface $(\sigma_0)_s$ is determined by the surface tension[1]:

$$(\sigma_0)_s \sim 4\Gamma/D_0 \tag{17}$$

while the effective $(\sigma_0)_m$ must take into account the effects of the average tensile stress S[39] and of the strain hardening. Then we can write:

$$(\sigma_0)_m \sim \beta S - \sigma_B(\text{or}) \tag{18}$$

where $\sigma_B(\text{or})$ is the back-stress, depending on the strain hardening and thus on the preorientation. The effective $(\sigma_0)_m$ defined in this way is that portion of the hydrostatic tension available to drive the non-Newtonian viscous flow in the active zone. Now (16) can be rewritten as:

$$\nabla\sigma_0 \sim 2[\beta S - \sigma_B(\text{or}) - 4\Gamma/D_0]/D_0 \tag{19}$$

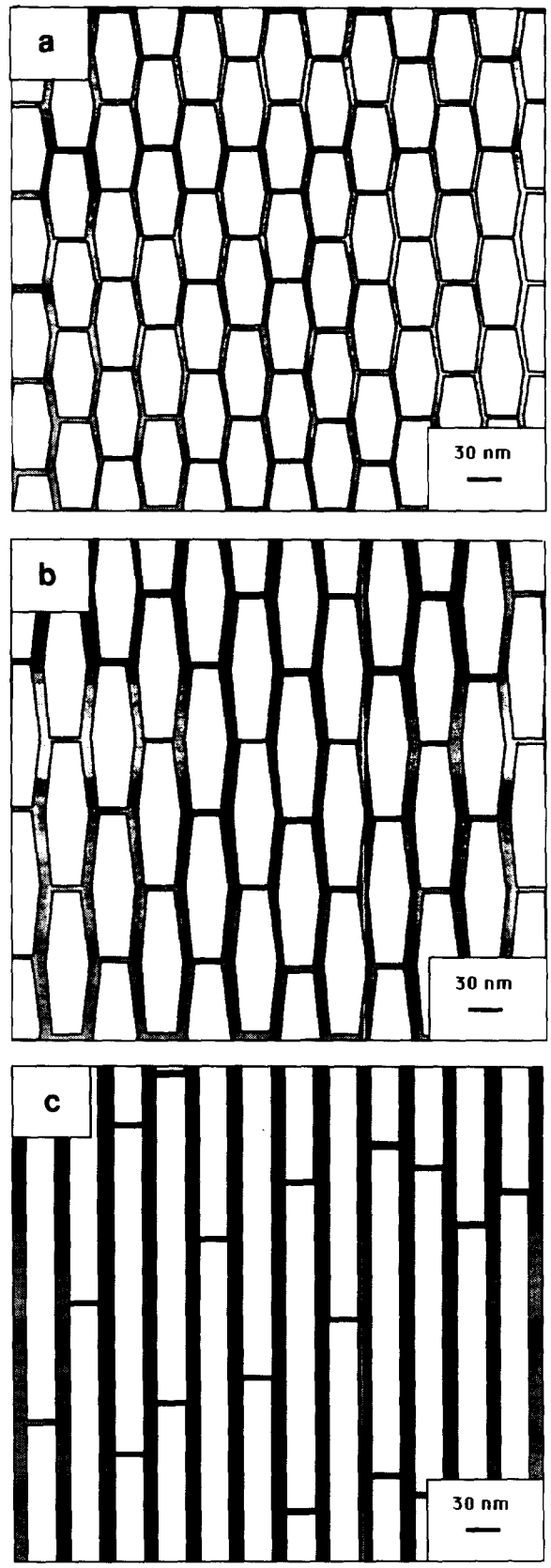

Figure 10 Idealized craze morphology showing cross-tie fibrils in oriented sample: (a) craze in perpendicular sample; (b) craze in unoriented sample; (c) craze in parallel sample

It is easy to check that $\nabla\sigma_0$ has a maximum at a corresponding value D_0^* that is given by:

$$[S - \sigma_B(\text{or})/\beta] = 8\Gamma/\beta D_0^* \tag{20}$$

Equation (20) is the equivalent of (15) in the case where

the back-stress caused by preorientation is not negligible in the fibril growth. In this case, instead of S_c being constant, the term $(S_c - \sigma_B(or)/\beta)$ must be a constant. Therefore S_c must increase with increasing parallel preorientation, to balance the corresponding increase in σ_B, in agreement with the experimental observations.

Statistics of craze nucleation, local craze breakdown and fracture

Preoriented film samples were prepared from the same filtered solution of PS in toluene and they were strained at room temperature with a strain rate of about $5 \times 10^{-6}\ s^{-1}$ in the directions parallel to and perpendicular to the orientation axis. Following the procedure first described by Yang and coworkers[29], the deformation was periodically interrupted for a very short time (2–3 min) in order to observe the sample at a magnification of 100× with an optical microscope using transmitted and reflected light.

As every sample contained approximately 50–60 diamond regions in which the evolution of the oriented film could be observed, good statistics for the craze nucleation, local fibril breakdown and catastrophic fracture could be obtained. We chose as the criterion for craze nucleation the presence of at least one observable craze. The local breakdown of a mature craze could be easily recognizable as a dark spot in reflected light. For fracture we arbitrarily required that a craze should have broken over at least one half of the diamond dimension. Of course, because of the low magnification used, the nucleation and breakdown criteria are not sensitive to the first stages of these phenomena. However they were sufficient to show large differences in the samples we considered. In the previously quoted work Yang and coworkers demonstrated that the presence and the size distribution of dust particles in the films were very important factors affecting the results. In our experiments no attempt to obtain ultra-clean samples was made other than filtering the solutions. In fact the manipulations needed to produce the oriented films, which required an exposure to a warm, dust-containing atmosphere for a relatively long time, would have made useless any further cleaning procedure.

The cumulative number fraction of the film diamond regions which had undergone craze initiation, p_c, local fibril breakdown, p_b, and catastrophic fracture, p_f, were detected at various strains during the tensile test. *Figure 11* shows p_c, p_b and p_f as functions of strain for the unoriented PS sample. Film regions that contained large dust particles or were poorly bonded to the grid were removed from consideration. In every tested sample the fracture curve p_f follows roughly the shape of the p_b curve, but is displaced to higher values of strain. This result is what one would expect if the fibril breakdown is the rate-controlling step in fracture[40].

From a plot like the one shown in *Figure 11* it is possible to estimate quantitatively the median strains ε_c, ε_b and ε_f defined by:

$$p_c(\varepsilon_c) = p_b(\varepsilon_b) = p_f(\varepsilon_f) = 0.5 \qquad (21)$$

These median strains for parallel and perpendicular samples *versus* ε_{or} are shown respectively in *Figures 12* and *13*. Our results for unoriented samples are in good agreement with those reported by Yang *et al.*[29]; the small remaining differences are most likely due to the different grid geometry. It is easy to conclude from the data that,

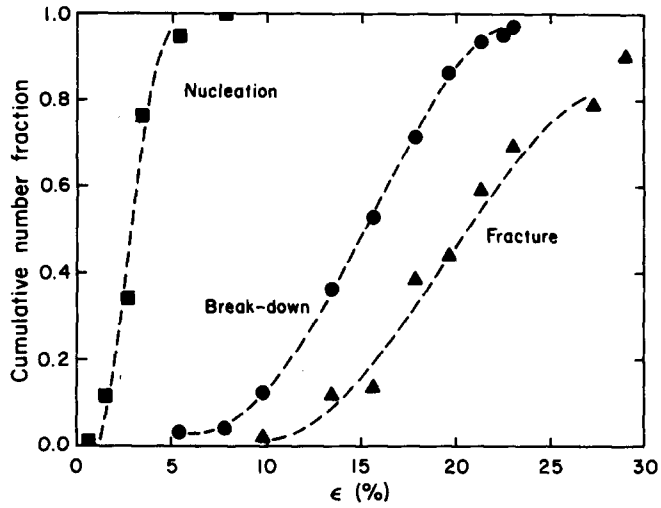

Figure 11 Plot of cumulative number fraction of the film diamond regions that had undergone craze nucleation (■), local fibril breakdown (●) and catastrophic fracture (▲) *versus* strain (%) in unoriented PS

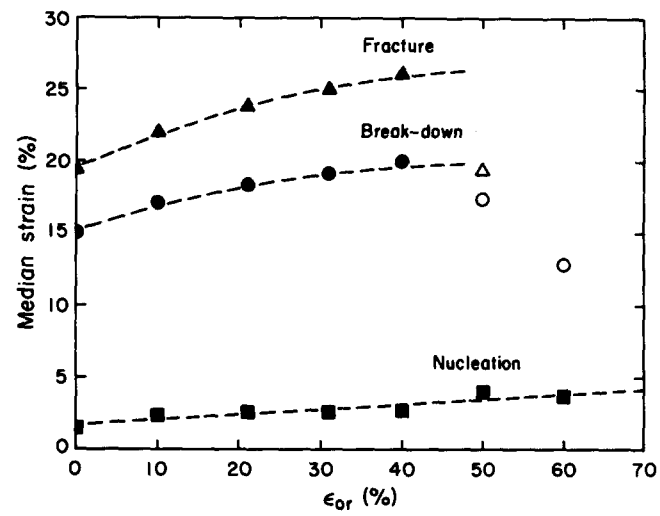

Figure 12 The median strains for craze nucleation (■), fibril breakdown (●) and fracture (▲) *versus* ε_{or} (%) in parallel samples. The open symbols (△, ○) represent data taken in samples in which the breakdown of the grids had occurred

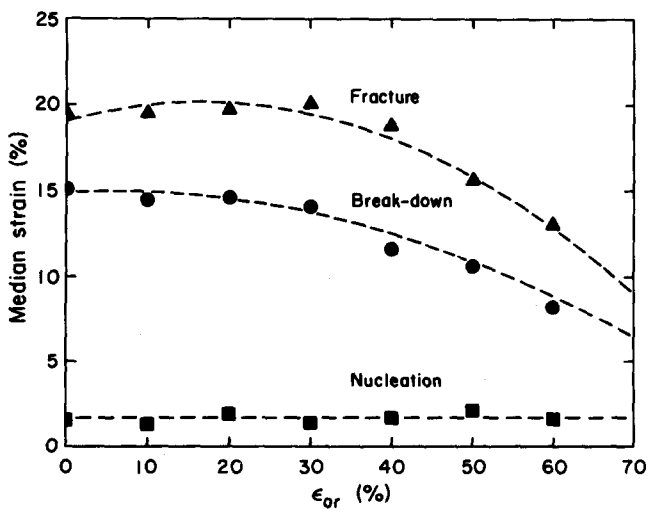

Figure 13 The median strains for craze nucleation (■), fibril breakdown (●) and fracture (▲) *versus* ε_{or} (%) in perpendicular samples

whereas the crazing strain ε_c is not strongly affected by the orientation and stays approximately constant in perpendicular samples while slightly increasing in parallel ones (in accord with the expected increase in the crazing stress), the breakdown and fracture strains ε_b and ε_f have a noticeable dependence on the orientation. As one could expect ε_b and ε_f decrease in perpendicular crazes and increase in parallel crazes with the exceptions of the two points obtained for $\varepsilon_{or} \geqslant 50\%$. These two points are not very meaningful because they come from data taken when the copper grids had reached their ultimate tensile strain and had begun to fracture at several points.

The statistics of craze fibril breakdown in unoriented PS[29] have been found to follow a Weibull distribution[41] when the new parameter ε_p, called 'plastic' strain, and defined as:

$$\varepsilon_p = \varepsilon - \varepsilon_c \tag{22}$$

is introduced. The Weibull expression for the probability of local fibril breakdown is the following:

$$p_b(\varepsilon_p) = 1 - \exp[-V_0 \varepsilon_p (\varepsilon_p/\varepsilon_w)^{\rho_w}/(\lambda_{cr} - 1)] \tag{23}$$

where p_b is the cumulative number fraction of diamond regions in which a local fibril breakdown occurred, V_0 is the initial film volume in a diamond region, and ρ_w and ε_w are, respectively, the Weibull modulus and the Weibull scale parameter, which have been demonstrated to be independent of the size of the samples[29]. Taking into account that all the samples came from the same solution, and then they have the same initial thickness, the initial volume V_0 of PS in a undeformed diamond region should be considered constant and then equation (23) can be rewritten as:

$$\ln\{\ln[1/(1 - p_b(\varepsilon_p))]\}$$
$$= (\rho_w + 1)\ln \varepsilon_p + [\ln V_0 - \ln(\lambda_{cr} - 1) - \rho_w \ln \varepsilon_w] \tag{24}$$

from which the Weibull modulus ρ_w and the scale parameter ε_w can be determined respectively from the slope and the y intercept of a plot $\ln\{\ln[1/(1 - p_b)]\}$ *versus* $\ln \varepsilon_p$, the so-called Weibull plot.

Figure 14 shows the Weibull plot for three samples with different degrees of orientation. The fit indicates that the Weibull distribution can describe the breakdown of

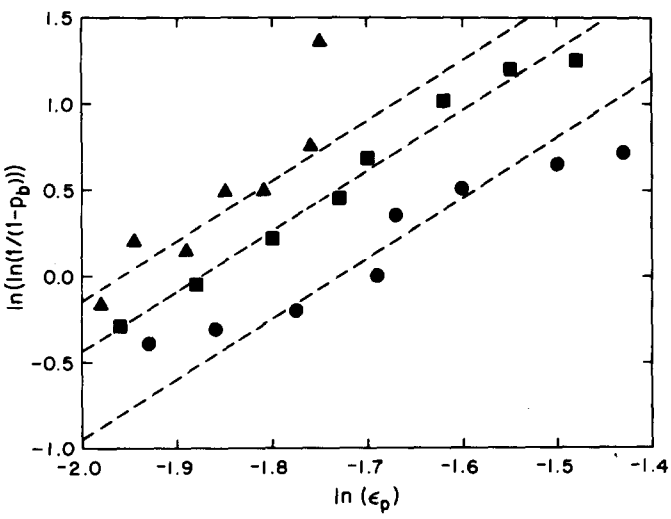

Figure 14 Weibull plot of the craze breakdown data: (▲) perpendicular sample ($\varepsilon_{or} \sim 30\%$); (■) unoriented sample; (●) parallel sample ($\varepsilon_{or} \sim 30\%$)

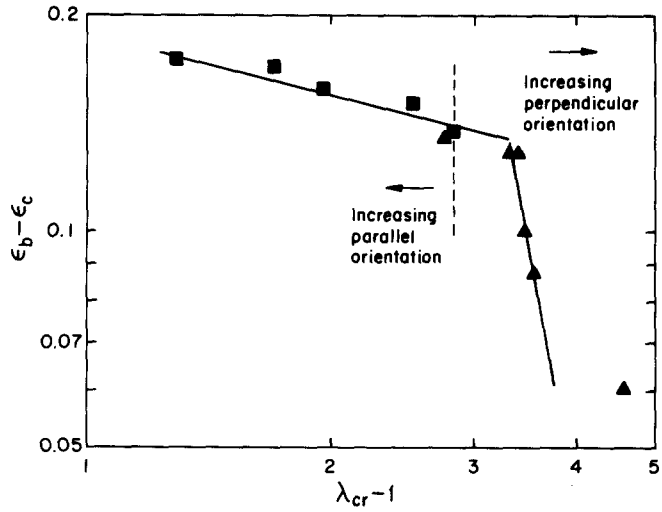

Figure 15 Logarithmic plot of the craze fibril stability parameter $(\varepsilon_b - \varepsilon_c)$ *versus* $(\lambda_{cr} - 1)$: (■) parallel samples; (▲) perpendicular samples. The two straight lines are included as guides to the eye

crazes in oriented samples. *Figure 14* shows also that the slope of the three straight lines can be considered constant, i.e. that the Weibull modulus ρ_w is independent of the orientation. The physical meaning of ρ_w is not extremely intuitive and comes from the definition[29]:

$$\Lambda = (\varepsilon_p/\varepsilon_w)^{\rho_w} \tag{25}$$

where Λ is the 'seed' density, including dust particles and intrinsic weak spots, relative to the fibril breakdown. In general terms ρ_w is interpreted as representing the distribution of effectiveness of the breakdown seeds. In our samples ρ_w has a value of approximately 3, which is the same as was found by Yang and coworkers in those samples of their's from which dust was not rigorously removed[29].

The physical meaning of ε_w, which appears to be the parameter predominantly influenced by the orientation, is much simpler. For samples of constant initial volume V_0, ε_w is proportional to $(\varepsilon_b - \varepsilon_c)$, the so-called 'fibril stability' parameter, which can be considered an indicator of the breakdown resistance of the craze fibrils. Yang and coworkers[29] developed a microscopic model for the fibril breakdown, later improved by Kramer and Berger[40], which involved the stability parameter. They derived the following expression:

$$\varepsilon_b - \varepsilon_c = \frac{[\rho_w(\lambda_{cr} - 1)\ln 2]^{1/\rho_w}}{[P_{sd}(S_1) n_f V_0]^{1/\rho_w}} \tag{26}$$

where $P_{sd}(S_1)$ is the probability that strands in a given fibril will break or disentangle at a craze stress S_1 corresponding to a plastic strain $\varepsilon_p = 1$ and n_f is the number of fibril elements (total number of entanglement transfer elements in the fibrils) formed from a unit risk volume $V = V_0 \varepsilon_p/(\lambda_{cr} - 1)$.

Although all the parameters in (26) can, in principle, be calculated[40], a simpler approach is followed here. We assume that the orientation dependence of the parameters $P_{sd}(S_1)$ and n_f is such that the overall λ_{cr} dependence of fibril stability $\varepsilon_b - \varepsilon_c$ is a power law in $(\lambda_{cr} - 1)$ so that (26) can be rewritten as:

$$\varepsilon_b - \varepsilon_c = F(\lambda_{cr} - 1)^{\alpha} \tag{27}$$

where both F and α are constant.

Figure 15 is a logarithmic plot of $(\varepsilon_b - \varepsilon_c)$ *versus*

($\lambda_{cr} - 1$) in which the λ_{cr} values are those computed in the previous section, assuming that the difference in strain rate in the two sets of experiments could not affect dramatically the extension ratio values[40]. Two separate linear regions exist with a sharp transition between them. Data from perpendicular samples with $\lambda_{or} > 1.3$ exhibit a much stronger dependence on λ_{cr}. This result indicates that a different mechanism of craze breakdown is active in the highly oriented perpendicular samples.

At the moment the exact reason for this rapid decrease in fibril stability with perpendicular orientation is not obvious. It may be caused, for instance, by an increase in chain scission and/or disentanglement within the drawing fibril due to the higher values of true stress accompanying the increase in λ_{cr}. What is clear, however, is that this rapid decrease in fibril stability with perpendicular orientation is responsible for much of the 'brittleness' observed in macroscopic tests on such samples.

CONCLUSIONS

The conclusions of our investigations may be summarized as follows:

The assumption that $\lambda_{cr} \sim \lambda_{max}$ is still valid in oriented PS and the experimental values of λ_{cr} are in good agreement with those inferred from the entanglement network of the polymer.

In highly preoriented parallel samples shear deformation zones growing at the edges of crazes have been observed, indicating a craze to shear transition above $\lambda_{or} \sim 1.4$.

While D, the average diameter of the craze fibrils, increases in parallel samples and decreases in perpendicular ones, the fibril spacing D_0 does not depend on the preorientation.

The presence and distribution of the cross-tie fibrils inside the crazes strongly depend on the preorientation, with higher density of cross-tie fibrils observed in perpendicular crazes and a lower density of cross-tie fibrils in parallel crazes.

A modification of the standard model of craze growth has been proposed, accounting for the effects of the strain hardening during the flow of polymeric material at the craze–bulk interface. The variations of the craze stress S_c can be qualitatively justified by this model.

Data from fragility tests in oriented samples demonstrate that fibril breakdown is the dominant step in craze fracture. The probability of fibril breakdown follows a Weibull distribution and the scale parameter ε_W, which, in our samples, is proportional to the stability parameter ($\varepsilon_b - \varepsilon_c$), appears to be the only parameter influenced by the orientation.

The fragility test data suggest that λ_{cr} is the main parameter affecting the craze stability, with craze stability decreasing strongly for higher λ_{cr}.

ACKNOWLEDGEMENTS

This research has been made possible by a grant from Montedipe (Italy) supporting the one-year-long stay of one of the authors (C.M.) in the Materials Science and Engineering Department of Cornell University. We also acknowledge use of the facilities of the Cornell Materials Science Center, which is funded by the NSF-DMR-MRL Program.

All the members of the Kramer group and the technical staff of MS&E are deeply thanked for their friendly collaboration and in particular Costantino Creton for his generous help during the experimental sessions.

The idea for pulling the copper grids along their diagonal to produce preoriented films grew out of discussions with Dr M. Dettenmaier while one of the authors (E.J.K.) was on sabbatical leave at the University of Mainz, made possible by a Senior US Scientist Award of the Alexander von Humboldt Stiftung.

REFERENCES

1 Kramer, E. J. *Adv. Polym. Sci.* 1983, **52/53**, 1
2 Berry, J. P. *J. Polym. Sci.* 1961, **50**, 313
3 Murray, J. and Hull, D. *Polymer* 1969, **10**, 451
4 Hull, D. *J. Mater. Sci.* 1970, **5**, 537
5 Kambour, R. P. *J. Polym. Sci. Macromol. Rev.* 1973, **7**, 1
6 Beahan, P., Bevis, M. and Hull, D. *Phil. Mag.* 1971, **24**, 1267
7 Brown, H. R. and Ward, I. M. *Polymer* 1973, **14**, 469
8 Doyle, M. J., Maranci, A., Orowan, E. and Stork, S. T. *Proc. R. Soc.* (*A*) 1972, **329**, 137
9 Rabinowitz, S. and Beardmore, P. *Crit. Rev. Macromol. Sci.* 1972, **1**, 1
10 Broutman, L. J. and McGarry, F. J. *J. Appl. Polym. Sci.* 1965, **9**, 609
11 Curtis, J. W. *J. Phys.* (*D*) *Appl. Phys.* 1970, **3**, 1413
12 Retting, W. *Colloid Polym. Sci.* 1975, **253**, 852
13 Jones, T. T. *Pure Appl. Chem.* 1976, **45**, 39
14 Gotham, K. V. and Scrutton, I. N. *Polymer* 1978, **19**, 341
15 Puttik, K. E. *J. Phys.* (*D*) *Appl. Phys.* 1978, **11**, L69
16 Lindsay, S. M., Hartley, A. J. and Sheperd, I. W. *Polymer* 1976, **17**, 501
17 Hennig, J. *Kunststoffe* 1967, **57**, 385
18 Robertson, R. and Buenker, R. J. *J. Polym. Sci.* (*A*) 1964, **2**, 4889
19 Wright, H., Faraday, C. S. N., White, E. F. T. and Treloar, L. R. G. *J. Phys.* (*D*) *Appl. Phys.* 1971, **4**, 2002
20 Beardmore, P. and Rabinowitz, S. *J. Mater. Sci.* 1975, **10**, 1763
21 Farrar, N. R. and Kramer, E. J. *Polymer* 1981, **22**, 691
22 Donald, A. M. and Kramer, E. J. *J. Polym. Sci., Polym. Phys. Edn.* 1982, **20**, 899
23 Donald, A. M. and Kramer, E. J. *J. Mater. Sci.* 1982, **16**, 2967
24 Donald, A. M. and Kramer, E. J. *Polymer* 1982, **23**, 461
25 Donald, A. M. and Kramer, E. J. *J. Mater. Sci.* 1982, **17**, 1871
26 Brown, H. R. *J. Polym. Sci., Polym. Phys. Edn.* 1983, **21**, 483
27 Yang, A. C. M. and Kramer, E. J. *J. Polym. Sci., Polym. Phys. Edn.* 1985, **23**, 1353
28 Yang, A. C. M., Kramer, E. J., Kuo, C. C. and Phoenix, S. L. *Macromolecules* 1986, **19**, 2020
29 Yang, A. C. M., Kramer, E. J., Kuo, C. C. and Phoenix, S. L. *Macromolecules* 1986, **19**, 2010
30 Lauterwasser, B. D. and Kramer, E. J. *Phil. Mag.* (*A*) 1979, **39**, 469
31 Donald, A. M., Kramer, E. J. and Bubeck, R. A. *J. Polym. Sci., Polym. Phys. Edn.* 1982, **20**, 1129
32 Donald, A. M. and Kramer, E. J. *Polymer* 1982, **23**, 1183
33 Donald, A. M. and Kramer, E. J. *J. Mater. Sci.* 1981, **16**, 2677
34 Porod, G. *Kolloid Z.* 1951, **124**, 83
35 Porod, G. *Kolloid Z.* 1952, **125**, 109
36 Miller, P. and Kramer, E. J. Proc. 7th Int. Conf. on Yield, Deformation and Fracture of Polymers, The Plastics and Rubber Institute, London, 1988; *J. Mater. Sci.* in press
37 Miller, P. Ph.D. Thesis, Cornell University, 1988
38 Argon, A. S. *Phil. Mag.* 1973, **28**, 839
39 Fields, R. J. and Ashby, M. F. *Phil. Mag.* 1976, **33**, 33
40 Kramer, E. J. and Berger, L. L. *Adv. Polym. Sci.* 1989, **91/92**, 1
41 Weibull, W. *J. Appl. Mech.* 1951, **18**, 293